Supplementary Material

Using a Human Circulation Mathematical Model to Simulate the Effects of Hemodialysis and Therapeutic Hypothermia

Jermiah J. Joseph[1,2], Timothy J. Hunter[1,2], Clara Sun[1,2], Daniel Goldman[2], Sanjay R. Kharche[1,2*], Christopher W. McIntyre[1*]

A. Supplementary Sections and Table.

Section S1. Model components and equations.

Our model consists of three sub-models that are coupled to each other. The whole body circulation model [1] is presented in **Figure 1**, while the detailed kidney, dialyzer model [2,3], and the baroreflex models [4,5] are illustrated in **Figures S1, S2, and S3**. Unless otherwise stated, model parameters have been adapted from the original literature. Inter-model coupling was implemented as described in the literature [6]. The body circulation model's renal Windkessel representation was further developed in this study. Specifically, the original model's renal arteriolar and microvascular resistances were distributed into two parallel circuits as shown in **Figure S1**. Further, the capacitances were evenly distributed among the two parallel kidneys. In each kidney, the baseline inlet resistance was assigned a value 5 mmHg-s/ml, and each of the six microvascular resistances were assigned values 15 mmHg-s/ml. Concurrently, the baseline inlet capacitance was assigned a value 5 mL/mmHg, and each of the six microvascular capacitances were assigned values 1.2 mL/mmHg.

In the coupled model, any resistance with value over 0.1 mmHg-s/ml was assumed to be large. All large resistances (represented by R) were dynamically computed as functions of vessel radius (represented by r) and blood viscosity (represented by η) as:

$$R = \frac{8\eta l}{\pi r^4} \tag{S1}$$

where R is resistance, eta is blood viscosity, l is length of vessel, and r is radius. The radius was considered to depend on temperature as

$$r_{35.5} = r_{37.5} \times Q_{10}{}^{\beta(35.5-37.5)} \tag{S2}$$

where Q_{10} = 2.1 is a constant. In all small vessels (vessels with resistance more than 0.1 mmHg-s/ml), the shear stress was computed using the viscosity, flow, and vessel diameter.

In this study, we considered cardiac output (CO), systemic artery systolic and diastolic pressures, and heart rate (beats per minute) as clinically relevant outputs. The cardiac output was computed by summing the left ventricle outflow over one heart beat.

Time varying elastance $E(t)$, as a function of diastolic elastance E_d, and systolic elastance E_s of each chamber:

$$E(t) = E_d + \frac{E_s - E_d}{2}\ \alpha(t) \tag{S3}$$

where $\alpha(t)$ is the activation function, specific to each chamber:

$$\alpha_{ventricle}(t) = \begin{cases} 1 - \cos\left(\pi \dfrac{t - T_{av}}{T_{s,v}}\right) & , \quad T_{av} < t \leq T_{av} + T_{s,v} \\ 1 + \cos\left(2\pi \dfrac{t - (T_{av} - T_{s,v})}{T_{s,v}}\right) & , \quad T_{av} + T_{s,v} < t \leq T_{av} + \dfrac{3}{2}T_{s,v} \\ 0 & \end{cases} \tag{S4}$$

$$\alpha_{atrium}(t) = \begin{cases} 1 - \cos\left(\pi \dfrac{t}{T_{s,a}}\right) & , \ 0 < t \leq T_{s,a} \\ 1 + \cos\left(2\pi \dfrac{t - T_{s,a}}{T_{s,a}}\right) & , \ T_{s,a} < t \leq \dfrac{3}{2}T_{s,a} \\ 0 & \end{cases}$$

The atrio-ventricular time-delay $T_{av} = 0.2$ s, along with the ventricular systolic time duration $T_{s,v}$ and atrial systolic time duration $T_{s,a}$, all scale with $\sqrt{T}$ where T is the cardiac cycle duration (in seconds).

Table S1. Model resistance, compliance, and cardiac elastance parameters used to generate populations. Baseline parameters were obtained from the literature [1,7].

Resistances (mmHg-s/ml).	
Inlet resistance of upper body.	3.9
Inlet resistance of splanchnic.	3.0
Inlet resistance of lower limbs.	3.6
Inlet resistance of right kidney.	5.0
Inlet resistance of left kidney.	5.0
Inlet resistance for kidney microcirculation, 12 independent resistances in total (see Figure S1).	15.0
Outlet resistance for kidney microcirculation, 12 independent resistances in total (see Figure S1).	0.3
Compliances (ml/mmHg).	
Pulmonary arteries.	4.3
Pulmonary veins.	8.4
Systemic arteries.	2.0
Upper body.	8.0
Splanchnic.	55.0
Lower limbs.	19.0
Abdominal veins.	25.0
Inferior vena cava.	2.0
Superior vena cava.	15.0
Kidney inlet.	15
Kidney microcirculation, 12 independent compliances in total (see Figure S1).	1.25
Cardiac parameters.	
Left atrial diastolic elastance (elastance has unit mmHg/ml).	0.5.
Right atrial diastolic elastance.	0.3
Left ventricle diastolic elastance.	0.13
Right ventricle diastolic elastance.	0.07

|	
Left atrial systolic elastance.	0.6.
Right atrial systolic elastance.	0.74
Left ventricle systolic elastance.	2.5
Right ventricle systolic elastance.	1.3
Atrial (left and right) systolic activation time.	0.25 s.
Ventricle (left and right) systolic activation time.	0.37 s.
Atrial to ventricular conduction time.	0.19 s.
Intrinsic heart rate (beats per minute).	70.
Baroreflex parameter.	
G factor, sympathetic feedback strength, unitless.	0.8.

B. Supplementary figures.
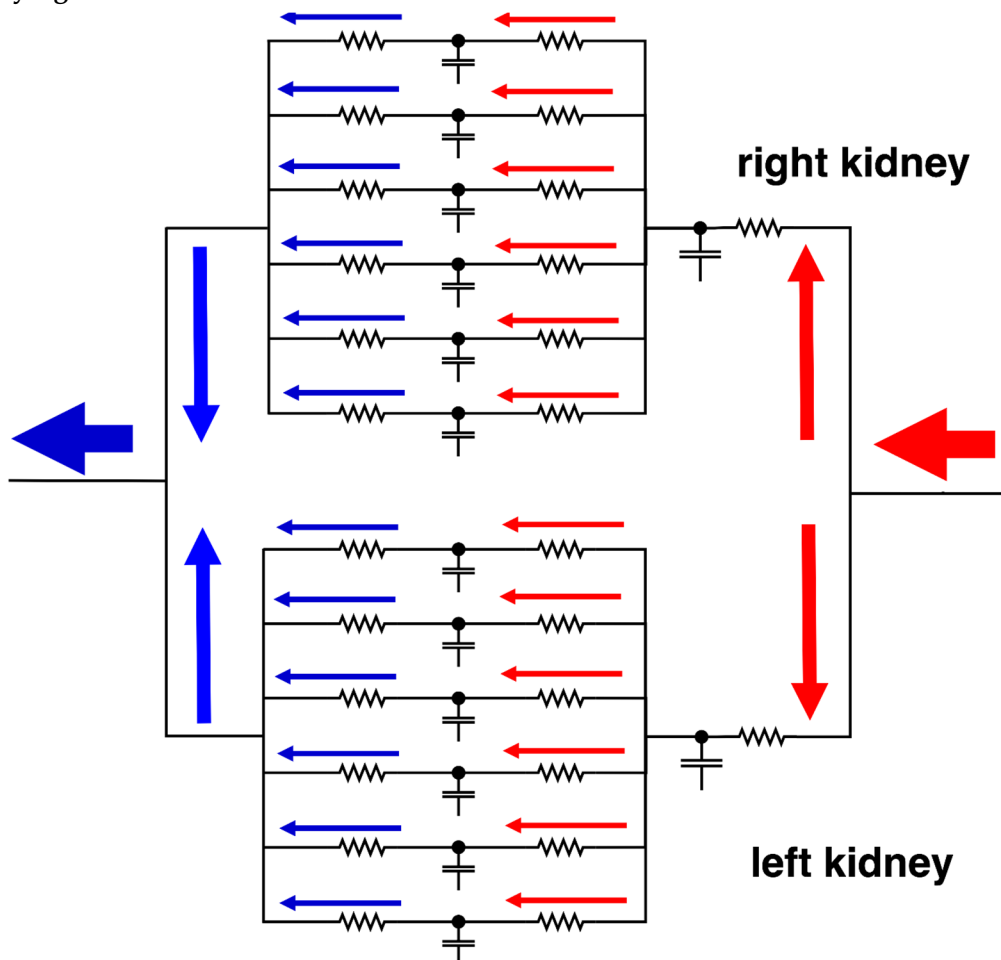
Figure S1. Schematic diagram of the detailed right-left kidneys' complex. Each kidney consists of six microvascular components, implemented as three element Windkessel models. Each component consists of two microvascular beds that is assigned two resistance values and one compliance value.

All resistances and compliances under baseline conditions were assumed to have the same value (see **Table S1** for parameter values).

**A**. Compartment used to simulate fluid exchange (dialyzer).
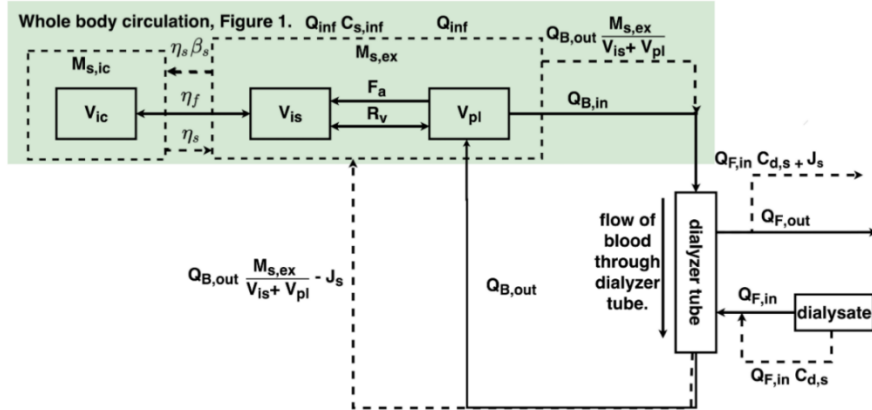

B. Description of acronyms in panel above.

Symbol.	Description.
	State and algebraic variables.
$M_{s,ic}$	Intracellular level of solute s.
$M_{s,ex}$	Extracellular level of solute s.
V_{ic}, V_{is}	Intracellular fluid volume, interstitial fluid volume respectively.
V_{ex}	Extracellular fluid volume.
V_{pl}	Plasma fluid volume .
F_a	Plasma filtration of arterial capillaries.
R_v	Reabsorption rate of venous capillaries.
	Relevant dialyzer constant parameters.
η_s	Mass-transfer coefficient for solute s.
J_s	Rate of solute s removal across the dialyzer.
β_s	Equilibrium ratio of the resting potential through cell membrane of solute s.
Q_{inf}	Filtration rate of replacement fluid.
Q_f	Dialysate flow rate, ultrafiltration rate.
$C_{d,s}$	Concentration of solute s in dialysate.

Figure S2. Schematic of the dialysis unit adapted from the literature. Further details including baseline parameter values used in this work can be found in Coli and Ursino [2,3,8] and Lim et al. [6].
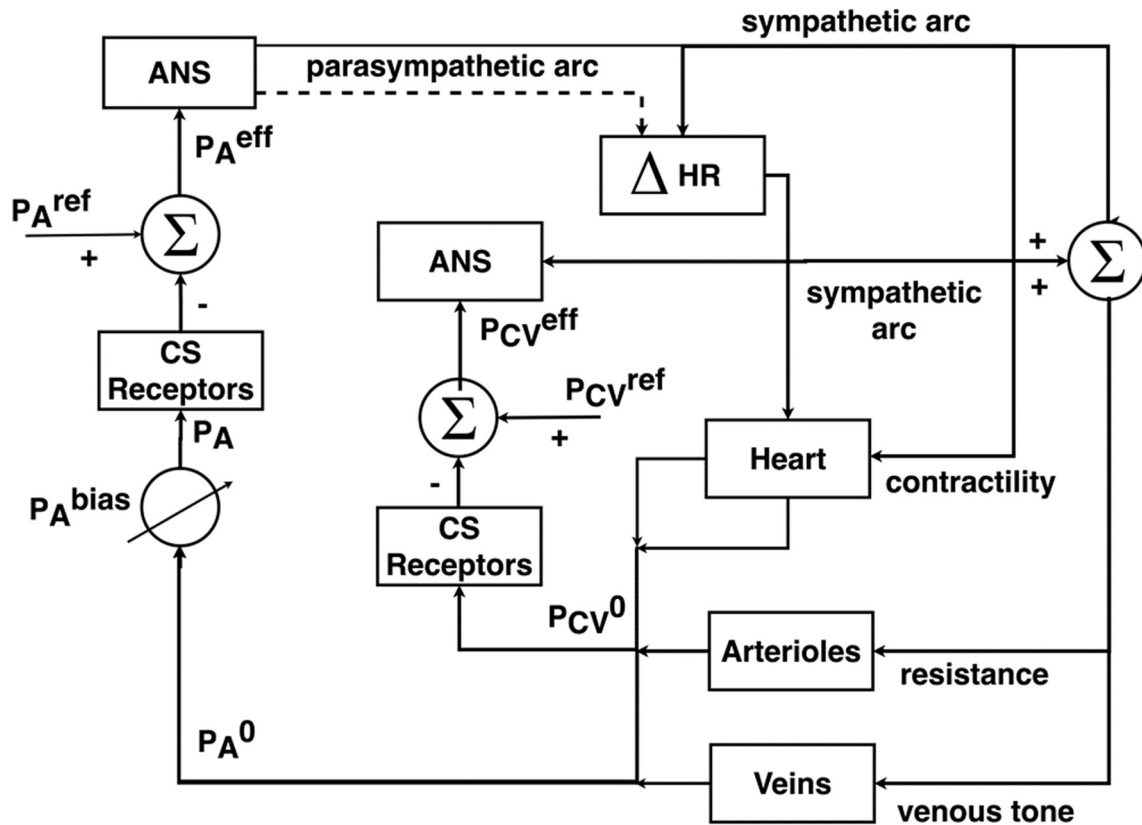
	Variables.
ANS	Autonomic nervous system.
P_A	Arterial blood pressure.
P_{CV}	Central venous blood pressure.
P_{CV}^0	Central venous instantaneous pressure.
P_A^{eff}	Effective pressure deviation.
P_A^{ref}	Arterial pressure reference.
P_A^{bias}	Time averaged arterial pressure.
P_A^0	Arterial instantaneous pressure.
ΔHR	Change in heart rate.

Figure S3. Schematic of the baroreflex sub-model adapted from Lin et al. [7].
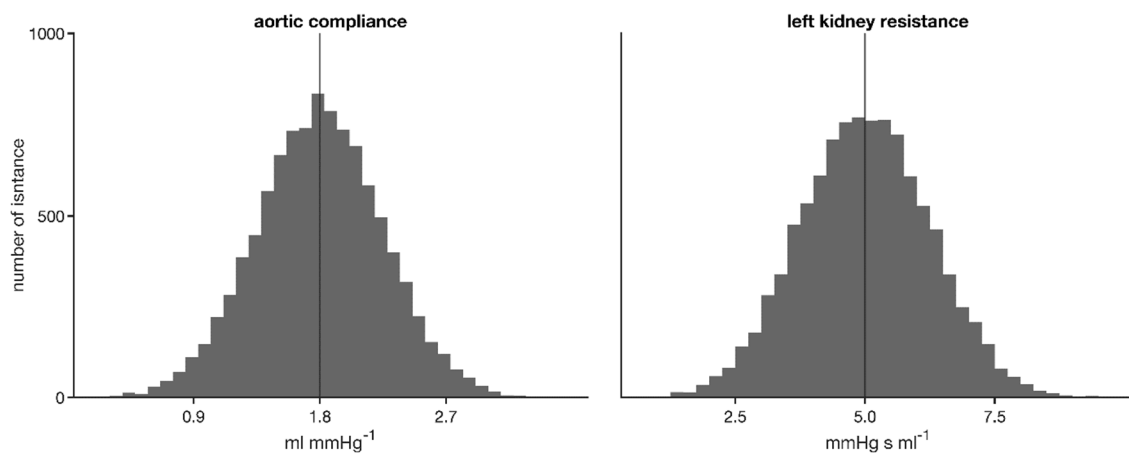
Figure S4. Representative parameter Gaussian distributions in the baseline model population (see **Figure 2**, main manuscript) where mean values are taken from the unperturbed model, and a coefficient of variation of 0.25 is used to generate the population. Left panel shows distribution of aortic compliance, and right panel shows distribution of left kidney inlet resistance.
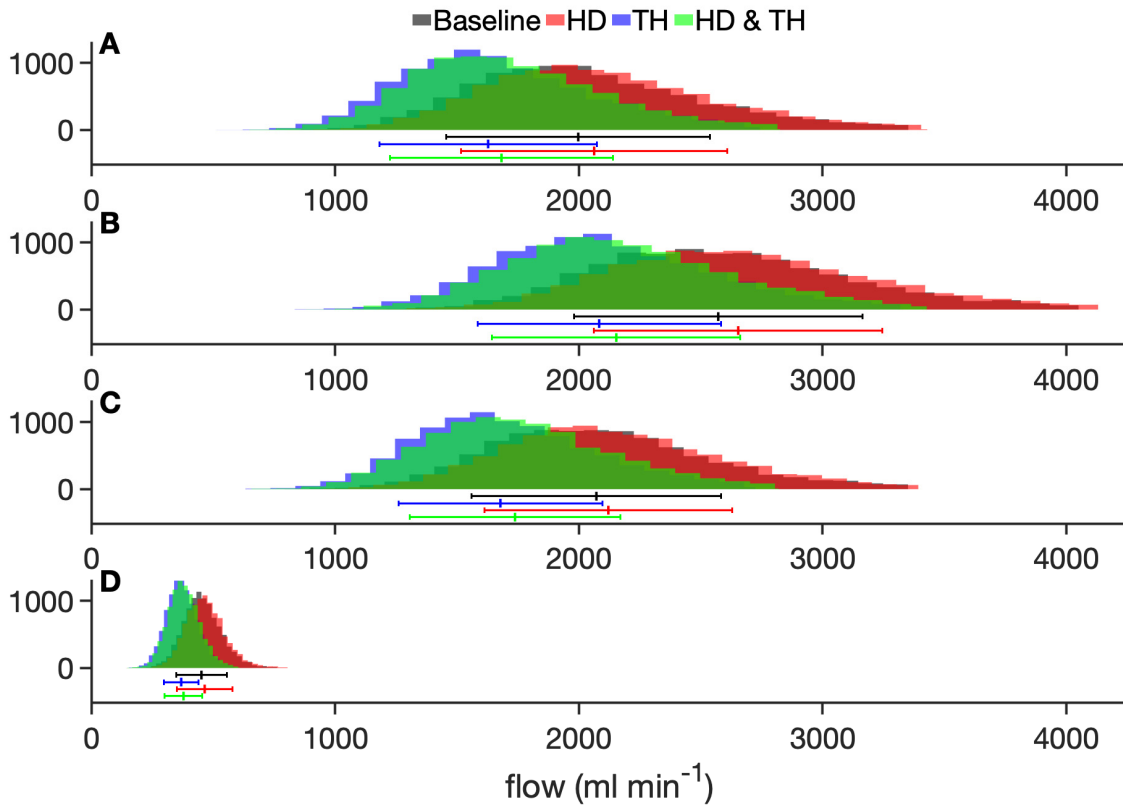
Figure S5. Distribution of flows in model organs under baseline (grey), hemodialysis (red), therapeutic hypothermia (blue), and simultaneous hemodialysis with therapeutic hypothermia (green). Top row: upper body; second row: splanchnic; third row: lower body; bottom row: two kidney complex. This illustration accompanies **Figures 2** and **3** in the main manuscript.
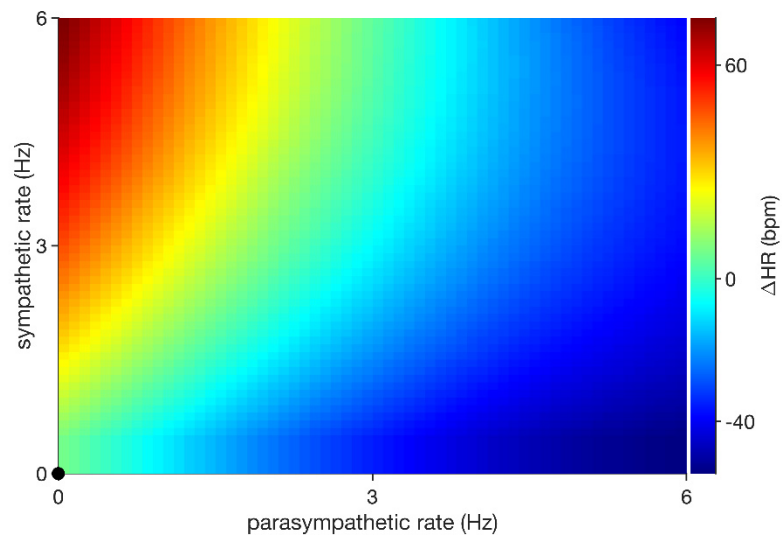
Figure S6. Baroreflex control of heart rate by the parasympathetic and sympathetic tone mechanisms. The control value is shown by the black circle in the bottom left hand corner of the panel. Both parasympathetic (horizontal axis) and sympathetic (vertical axis) rate values are shown after subtracting the baseline value. See **Table S1** for parameter values.
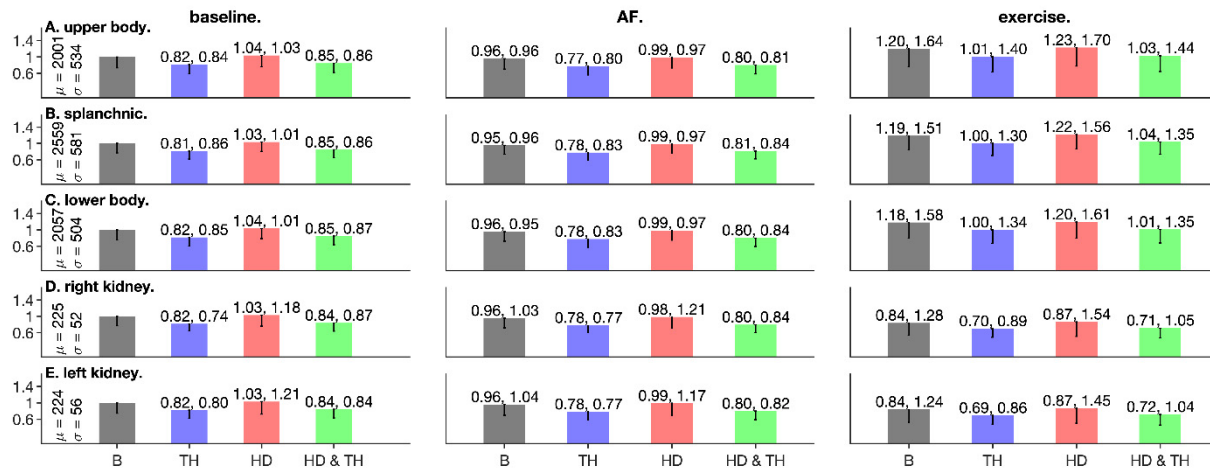
Figure S7. Blood flow under baseline (left column), AF (middle column), and exercise (right column) conditions. All data are normalized to the baseline values of the left panel.
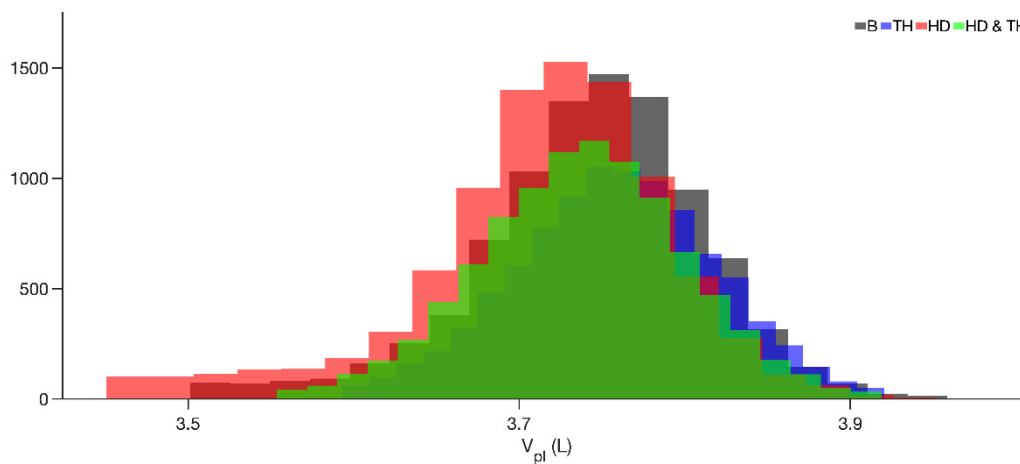
Figure S8. Population distributions of intracellular volume (left panel), interstitial volume (middle panel), and plasma volume (right panel). See **Figures 2 and 3** and related text for details.

References

1. Heldt, T.; Shim, E.B.; Kamm, R.D.; Mark, R.G. Computational modeling of cardiovascular response to orthostatic stress. *J. Appl. Physiol.* **2002**, *92*, 1239–1254.
2. Ursino, M.; Coli, L.; Brighenti, C.; Chiari, L.; de Pascalis, A.; Avanzolini, G. Prediction of solute kinetics, acid-base status, and blood volume changes during profiled hemodialysis. *Ann. Biomed. Eng.* **2000**, *28*, 204–216.
3. Coli, L.; Ursino, M.; Dalmastri, V.; Volpe, F.; La Manna, G.; Avanzolini, G.; Stefoni, S.; Bonomini, V. A simple mathematical model applied to selection of the sodium profile during profiled haemodialysis. *Nephrol Dial. Transplant.* **1998**, *13*, 404–416.
4. deBoer, R.W.; Karemaker, J.M.; Strackee, J. Hemodynamic fluctuations and baroreflex sensitivity in humans: A beat-to-beat model. *Am. J. Physiol.* **1987**, *253*, H680–H689.
5. Lin, C.L.; Tawhai, M.H.; Hoffman, E.A. Multiscale image-based modeling and simulation of gas flow and particle transport in the human lungs. *Wiley Interdiscip. Rev. Syst. Biol. Med.* **2013**, *5*, 643–655.
6. Lim, K.M.; Choi, S.W.; Min, B.G.; Shim, E.B. Numerical Simulation of the Effect of Sodium Profile on Cardiovascular Response to Hemodialysis. *Yonsei Med. J.* **2008**, *49*, 581–591.
7. Lin, J.; Ngwompo, R.F.; Tilley, D.G. Development of a cardiopulmonary mathematical model incorporating a baro-chemoreceptor reflex control system. *Proc. Inst. Mech. Eng. Part H J. Eng. Med.* **2012**, *226*, 787–803.
8. Coli, L.; Ursino, M.; De Pascalis, A.; Brighenti, C.; Dalmastri, V.; La Manna, G.; Isola, E.; Cianciolo, G.; Patrono, D.; Boni, P.; et al. Evaluation of intradialytic solute and fluid kinetics. Setting Up a predictive mathematical model. *Blood Purif* **2000**, *18*, 37–49, doi:10.1159/000014406.